



Improved hole repairing algorithm for livestock point clouds based on cubic B-spline for region defining

Wen Zhikun^a, Yu Jincheng^a, Yin Ling^{a,b,*}, Zhang Sumin^a, Cai Yehao^a, Liu Caixing^{a,c}, Tian Xuhong^a

^a College of Mathematics and Informatics, South China Agricultural University, Guangzhou 510642, China

^b National Engineering Research Center for Swine Breeding Industry, Guangzhou 510642, China

^c Guangdong Wens Breeding Swine Technology Co., Ltd, XinXing 527400, China

ARTICLE INFO

Keywords:
 Cubic b-spline curve
 Holes repairing
 Least squares method
 Region defining

ABSTRACT

Because of the occlusion of the railings, the collected animal point clouds become fragmentary and have the large holes. The incomplete point clouds have a great impact on body size measurements of pigs. This paper presents an improved hole repairing algorithm based on cubic B-spline curve for region defining. Meanwhile, by applying approximation fitting and interpolation based on cubic B-spline curve, we can repair the holes of the pig point clouds after slicing longitudinally in the mid-axis plane of the pig body point clouds. In the experiment, comparisons were made among polar coordinate transformation algorithm, surface fitting algorithm, triangulation algorithm, and the algorithm proposed by us to verify hole repairing effect and estimation accuracy of abdominal circumference. The results show that we have proposed an algorithm with a better repairing effect and a higher accuracy in the abdominal circumference measurement of pigs.

0. Introduction

Phenotypic value selection is a method commonly used in pig breeding [1]. Body size is a set of quantitative indices that describe the external features of pigs at a specific stage of weight, reflecting the characteristics of pig breeds, growth and development. Pig body size traits have long been manually measured, during the process of which many problems are likely to arise, e.g., livestock driving stress, poor accuracy in manual measurement, difficulty in measuring complex traits, and low production efficiency. With the growing scale of pig breeding and pig farming industry, there is an urgent need to establish non-contact intelligent solutions that are more efficient and accurate [2].

Two methods are mainly employed in 3D point cloud acquisition: fixed acquisition method and portable acquisition method [3–6]. The fixed acquisition device restricts the livestock in the channel with railings where it can walk freely to obtain the point clouds, while the portable type adopts the handheld method by fixing the collection device close to the livestock to get an adjustable angle, so that the point cloud acquisition is automatically completed. As for fixed acquisition method, railings are usually used to restrict the activity scope of the

livestock and prevent damage to the data collection equipment [7]. However, the railings can block the acquisition of livestock point clouds and cause large holes, dividing the point clouds into multiple parts and destroying its integrity. The point clouds with mass hollows will affect the measurement of thoracic circumference, rump circumference, and abdominal circumference of pigs, as well as point cloud segmentation and skeleton extraction [8]. In short, point cloud holes affect both the visualization of the model and the post-processing of the point clouds. Since there are various types of point clouds holes, many scholars have conducted extensive research on their repair [9–13]. Currently, many methods are available for repairing discrete point cloud holes: The hole repairing algorithm based on the projection characteristic plane, that is, the entire point cloud data is parameterized or projected onto the plane for processing. This method is suitable for repairing small-scale holes, curved surfaces with few changes in curvature characteristics, and regular shapes [14]. However, it tends to underperform in repairing holes with rich details. Furthermore, three-dimensional space direct hole repair methods, such as the use of the repairing algorithm based on latitude-longitude grid [15], moving least squares interpolation method to fill and repair the hole areas by surface fitting [16–19], bidirectional waveform method to repair island-like holes have also been developed

* Corresponding author at: College of Mathematics and Informatics, South China Agricultural University, Guangzhou 510642, China.
 E-mail address: yin_ling@scau.edu.cn (Y. Ling).

[20,21]. Triangular mesh hole repairing algorithm triangulates the surface of the hole area to form a hole patch, which is stitched to the model hole area to realize hole repair [22–24]. This algorithm is suitable for defect hole repair in single connected regions. For the complex topological structure of missing regions, the algorithm time complexity is relatively high.

The existing hole repairing algorithms focus on repairing holes with small size, smooth edge and unobvious curvature variation. In this paper, the missing area caused by the railing is large and non-closed. Relatively speaking, the positions of the railings and the acquisition camera are not fixed, so the positioning information cannot be directly used to repair the hole. In this paper, we propose an improved hole repairing algorithm based on cubic B-spline curve for region defining. First, the least squares method is used to fit the mid-axis plane of the pigs. Then the pig body is longitudinally sliced and projected after the point cloud hole repair range is determined. Finally, the repair of the pig body point cloud is completed after approximation fitting and interpolation by using the cubic B-spline curve, and the point clouds are down-sampled to balance the number of point clouds that have been repaired. In the experiment, the point cloud data of the target pigs and the point cloud data of different tetrapod animals were utilized for hole repair and abdominal circumference calculation; practicability and robustness of the algorithm were verified; comparisons were made among four algorithms, including the polar coordinate transformation algorithm, surface fitting algorithm, triangularization algorithm and the algorithm proposed in this paper.

1. Materials and methods

1.1. Experimental conditions

The experimental data include a point cloud data set of the target pigs in a free walking state collected in a pig farm and a standard dataset of tetrapod animal point clouds. The data acquisition environment of the pig farm is shown in Fig. 1: The data acquisition channel has 3 KinectV2 depth cameras to obtain the local point clouds from three different perspectives: left view, right view, and top view. After the data pre-processing such as point cloud denoising, registration and fusion, the global point cloud data of the target pigs was obtained [25–27]. The experimental data was collected from 20 target pigs in the breeding farm, and 4 groups of complete three-dimensional point clouds were collected for each target pig. In total, the point cloud data of 80 target pigs was obtained. The point cloud data sets of standard tetrapod are those of the standard dinosaur, horse, cow, dog, and puma provided by Princeton Model Net and the Large Geometric Model Archives at Georgia Institute of Technology.



Fig. 1. Data acquisition channel in the pig farm.

1.2. Improved hole repairing algorithm based on cubic B-spline curve

The specific process of the improved hole repairing algorithm based on cubic B-spline curve is shown in Fig. 3. Multiple KinectV2 cameras acquire local point clouds of the target pigs from three different angles. After point cloud denoising, registration and fusion, the global point cloud data of the target pigs was obtained [28,29], as is shown in Fig. 2. The least squares method plane fits the mid-axis plane of the pig back point clouds, divides the point cloud into the left and right parts, and calculates the hole area for the two parts respectively by using projection plane, and then slices along the body length and orders the slice data. Then, it performs cubic B-spline curve fitting and down-sampling to achieve hole repair.

1.2.1. Point cloud preprocessing

(1) Point cloud denoising

The data acquisition process is influenced by the external environment and equipment, and the point cloud data obtained contains a lot of noise, which affects the subsequent operations. Therefore, denoising is an important part of the point cloud preprocessing.

The point clouds with noise points usually fall into two categories. One is the long-distance outliers far away from the target point clouds, with their distribution being sparse and their random distributions as a small group of isolated points in a three-dimensional space. The distance-based area growth method can filter out the long-distance outliers. The other is the short-distance outliers close to the target point clouds, and the non-iterative dual-threshold denoising algorithm is used to remove the short-distance outliers [30].

(2) Point cloud registration and fusion

Three depth cameras capture local point clouds from different perspectives in three directions: top view, left view, and right view. Registration and fusion realize the conversion from point clouds obtained from various angles to the same coordinate system through rotation and translation [31–36].

In this paper, a pig body point cloud registration algorithm based on a still cuboid is used. The standard cuboid with its length (60cm), width (50cm) and height (50cm) are used as the calibration object and placed in the point cloud acquisition channel. The relationship between the coordinate system of each camera and the corresponding position is shown in Fig. 4 (a). The above camera coordinate system is used as the world coordinate system, and it is registered pairwise with the coordinate systems on both sides. The PCL [37] random sampling consensus algorithm is used to extract the point clouds of the calibration object plane in the point clouds captured by the camera at each angle, from which the four key points of the calibration object plane in the corresponding direction are determined, and the position of the calibration object plane in the world coordinate system is located through the key

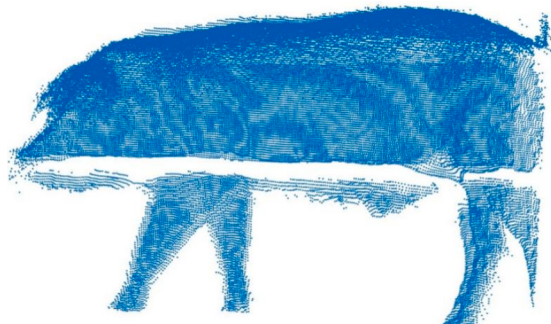


Fig. 2. Three-dimensional pig body projection with point cloud holes.

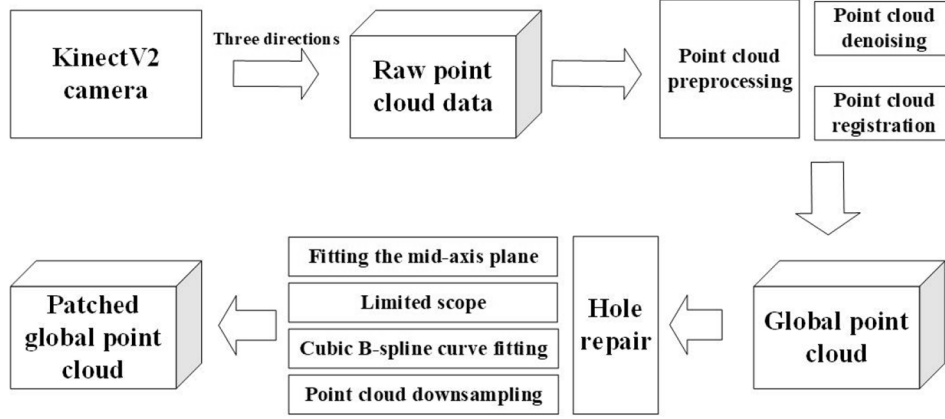


Fig. 3. Realization process of improved hole repairing algorithm based on cubic B-spline curve.

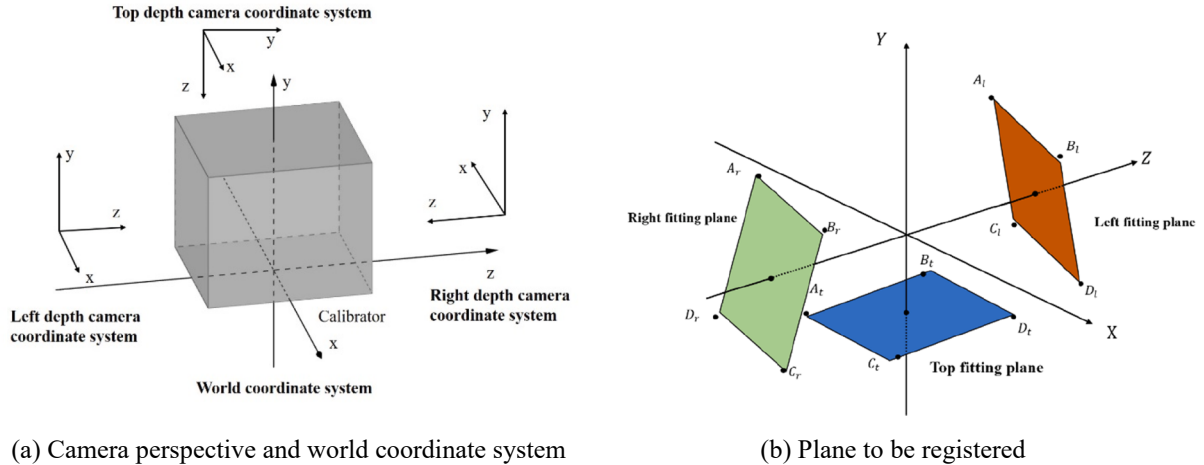


Fig. 4. Registration diagram of point clouds.

points, as is shown in Fig. 4 (b).

The two fitting planes that need to be registered are first transformed to the same pair of common points via translation, and then two rotations and alignments are performed respectively. The first rotation transformation makes the two fitting planes have a common edge, and then the second rotation transformation makes the two fitting planes completely vertical, and finally the two fitting planes completely restore the actual physical position relationship. The corresponding homogeneous transformation matrices R and T are obtained by two homogeneous rotations, and the coordinates are transformed into the same coordinate system according to formula (1).

$$\begin{bmatrix} x_1 \\ y_1 \\ z_1 \end{bmatrix} = R \begin{bmatrix} x_0 \\ y_0 \\ z_0 \end{bmatrix} + T = \begin{bmatrix} R_1R_2R_3 \\ R_4R_5R_6 \\ R_7R_8R_9 \end{bmatrix} \begin{bmatrix} x_0 \\ y_0 \\ z_0 \end{bmatrix} + \begin{bmatrix} t_x \\ t_y \\ t_z \end{bmatrix} \quad (1)$$

where R is the rotation transformation matrix, T is the translation vector, $[x_0y_0z_0]^T$ is the original coordinate to be registered, and $[x_1y_1z_1]^T$ is the coordinate after the corresponding transformation.

1.2.2. Hole repairing

After denoising and registration, the three-dimensional point clouds have long, narrow and open gap holes on both sides of the pig body, which makes the point cloud features of pig abdomen become obviously incomplete, as is shown in Fig. 2. Before repairing point cloud holes, the hole areas should be determined so as to reduce the impact of point clouds in irrelevant areas and reduce the amount of calculation.

(1) Fitting the mid-axis plane of the pig body

The pig body is symmetrical on the left and right sides. Finding the mid-axis plane can effectively divide the pig body point clouds into left side and right side, reducing the interference caused by the point clouds of either side during projection. Specifically, the least squares method fits the mid-axis plane: suppose the global point cloud data is $P = \{p_1, p_2, p_3, \dots, p_n\}$, where the point $p_i = (x_i, y_i, z_i)$. The general equation of the plane is computed as:

$$z = a_0x + a_1y + a_2 \quad (2)$$

For the point clouds $P(x_i, y_i, z_i)$, in order to make the plane closer to the point clouds, the minimum value of S is required.

$$S = \min \sum_{i=1}^n (a_0x_i + a_1y_i + a_2 - z_i)^2 \quad (3)$$

Satisfy the minimum of S to satisfy the formula (4)

$$\frac{\partial S}{\partial a_k} = 0, k = 0, 1, 2 \quad (4)$$

then

$$\begin{cases} a_0 \sum x_i^2 + a_1 \sum x_i y_i + a_2 \sum x_i z_i = \sum x_i z_i \\ a_0 \sum x_i y_i + a_1 \sum y_i^2 + a_2 \sum y_i = \sum y_i z_i \\ a_0 \sum x_i + a_1 \sum y_i + a_2 n = \sum z_i \end{cases} \quad (5)$$

By solving the above equations, the values of a_0, a_1, a_2 are obtained,

and the plane equation $z = a_0x_i + a_1y_i + a_2$ is obtained, which is the mid-axis plane to be fitted. In Fig. 5, the part in gray represents the fitting mid-axis plane.

(2) Delineation of the scope of hole repair

Fitting the mid-axis plane divides the global point clouds into two parts: the left side point clouds and the right side point clouds (referred to as left point cloud and right point cloud for short), which reduces the mutual interference of the point clouds on both sides, making it easier to determine the boundary. The left and right point clouds are respectively projected onto the XOY plane, and the missing point clouds obscured by the railings will have abrupt changes in the Y values between adjacent data points, thereby determining the position of the hole boundary. The point clouds are scattered and irregularly distributed, and the number of point clouds corresponding to a single point X coordinate value is small and disorderly, so the point cloud data with stable number and regular distribution can be obtained by block slicing.

Specifically, if we take the left point cloud as an example, let the left point cloud data be L , the number of point clouds is m , $L = \{l_1, l_2, l_3, \dots, l_m\}$, $l_i = (x_i, y_i, z_i)$, make XOY plane projection, the point set $L_p = \{lp_1, lp_2, lp_3, \dots, lp_n\}$, $lp_i = (x_i, y_i, 0)$ after projection. If we slice along the X axis, the number of slices is B , and the slice size is $slice$.

$$slice = \frac{\max(x_i) - \min(x_i)}{B} \quad (6)$$

The set of slice j points is expressed as $S_j = \{s_1, s_2, s_3, \dots, s_n\}$, $s_k = (x_k, y_k, 0)$, $x_k \in [\min(x_i) + (j - 1)*slice, \min(x_i) + j*slice]$, $j \in (1, 2, 3, \dots, B)$, sort the data points in S_j according to the y value, so that $\forall s_k \in S_j$, $y_{k+1} > y_k$, find out $\max(y_{k+1} - y_k)$, when $y_{t+1} - y_t = \max(y_{k+1} - y_k)$, $[y_{t+1}, y_t]$ is the railing area in the current slice which is recorded as $[b_{j1}, b_{j2}]$. Eq. (7) calculates the upper boundary L_{upper} of the railing relevant to the left point cloud, and the lower boundary L_{lower} .

$$\begin{cases} L_{upper} = \max(b_{j1}), j \in (1, 2, 3, \dots, B) \\ L_{lower} = \min(b_{j2}) \end{cases} \quad (7)$$

Similarly, the upper boundary R_{upper} and the lower boundary R_{lower} of the railing related to the right point cloud can be obtained. Formula (8) is used to calculate the upper boundary U and lower boundary D of the railing of the global point clouds. The position of the railing area is determined by the red line in Fig. 6, with different colors representing different slice areas.

$$\begin{cases} U = \max(L_{upper}, R_{upper}) \\ D = \min(L_{lower}, R_{lower}) \end{cases} \quad (8)$$

To determine the range of the abdominal point clouds, the left point clouds and the right point clouds should be evenly divided into four slices along the X axis, and the lowest point of the third slice is selected as the lower left boundary and the lower right boundary.

Specifically, if we take the left point clouds as an example, set the lower boundary of the abdomen to be fitted as L_a , set the number of slices $B = 4$, calculate the slice size according to formula (6), and the X-axis interval of the third slice is $[\min(x_i) + 2*slice, \min(x_i) + 3*slice]$, find the minimum y value of the point in the slice range, $L_a = \min(y_i)$, find

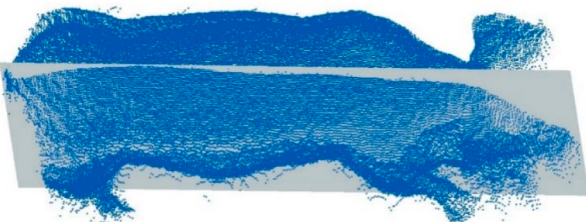


Fig. 5. Schematic diagram of fitting the mid-axis plane.

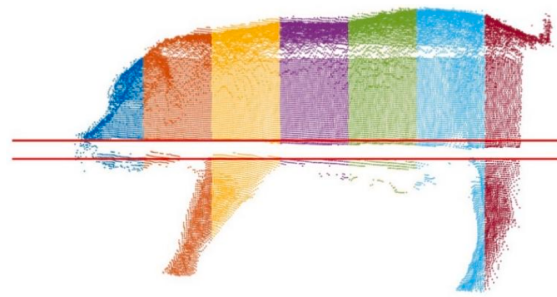


Fig. 6. Schematic diagram of slice projection.

the lower border of the abdomen of the right point cloud for R_a , Eq. (9) calculates the lowest point of the abdomen Down.

$$Down = \begin{cases} \min(L_a, R_a), |L_a - R_a| \leq 0.1, \\ \max(L_a, R_a), |L_a - R_a| > 0.1 \end{cases} \quad (9)$$

Add 0.1 to the upper boundary U of the railing position to get Top , and determine the repair range as $[Down, Top]$, where $Down$ is the lower boundary, and Top is the upper boundary. The area between the two red lines in Fig. 7 represents the repair scope determined.

(3) Improving the hole repair algorithm based on cubic B-spline curve

The point clouds in the area to be repaired is longitudinally sliced along the X axis; the slices are projected onto the YOZ plane; the projected point cloud are ordered, and the interpolation point density is set according to the effect to be repaired by using cubic B-spline curve for interpolation repair.

For the point clouds in the area to be repaired, $H = \{h_1, h_2, h_3, \dots, h_a\}$, $h_i = (x_i, y_i, z_i)$, the number of slices is $Blocks$, slice along the X axis, according to Eq. (10), the slice size is $slice$.

$$slice = \frac{\max(x_i) - \min(x_i)}{Blocks}, i \in (1, 2, 3, \dots, a) \quad (10)$$

Project the slice onto the YOZ plane, where the slice j is $Q_j = \{q_1, q_2, \dots, q_b\}$, $q_i = (x_i, y_i, z_i)$. Fig. 8 (a) represents the projection of the complete slice; Fig. 8 (b) represents the projection of the area to be repaired. At this stage, the point clouds in disorderly distribution should be ordered. The projection of the point cloud slice to be repaired from left to right shows a trend of progressive decrease before progressive increase, so the slice projection is first divided into the left part and the right part with the middle axis plane as the boundary, and then the left point clouds are sorted in a descending order, and the right point clouds are sorted in an ascending order. Accordingly, in the left point clouds, $\forall (z_{i+1} > z_i), y_{i+1} < y_i$, and in the right point clouds, $\forall (z_{i+1} > z_i), y_{i+1} > y_i$. Fig. 8 (c) represents the point cloud projection to be repaired after ordering.

For the sorted point clouds, a cubic B-spline curve method is used to

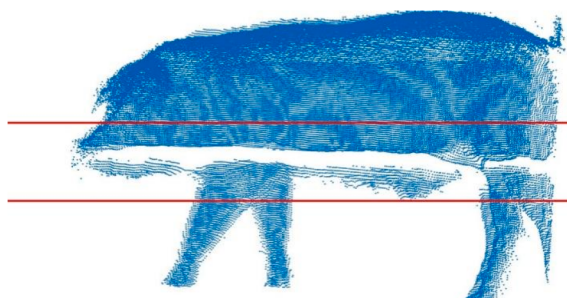


Fig. 7. Schematic diagram of the area to be repaired.

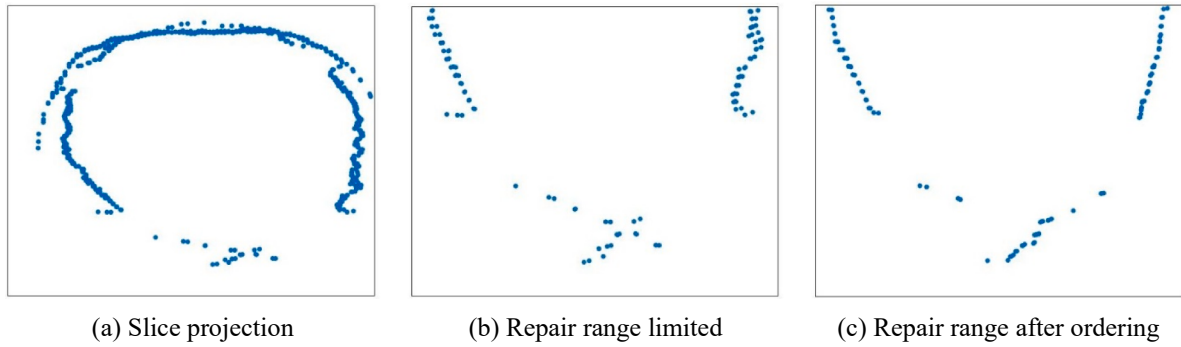


Fig. 8. Point cloud projection to be repaired.

repair the points, where the expression of the B-spline curve is:

$$P(t) = \sum_{i=1}^n P_i F_{i,k}(t) \quad (0 \leq t \leq 1) \quad (11)$$

where $P_i (i = 0, 1, 2, \dots, n)$ is a set of $n+1$ control points in space, $t = \{t_0, t_1, \dots, t_m\}$ are $m+1$ vectors, $F_{i,k}(t)$ is the basis function of the k -order or $k-1$ degree B-spline curve. The basis function of the B-spline curve is:

$$F_{i,k}(t) = \frac{1}{k!} \sum_{j=0}^{k-i} (-1)^j C_{k+1}^j (t+k-i-j)^k, \quad t \in [0, 1], i = 0, 1, 2, \dots, n \quad (12)$$

When $k=3$, there is the basis function of cubic B-spline curve:

$$\left\{ \begin{array}{l} F_{0,3}(t) = \frac{1}{6}(1-t)^3 \\ F_{1,3}(t) = \frac{1}{6}(3t^3 - 6t^2 + 4) \\ F_{2,3}(t) = \frac{1}{6}(-3t^3 + 3t^2 + 3t + 1) \\ F_{3,3}(t) = \frac{1}{6}t^3 \end{array}, t \in [0, 1] \right. \quad (13)$$

Substitute the basis function of the cubic B-spline curve into the expression of the B-spline curve, and the cubic B-spline curve equation is obtained:

$$P(t) = P_0 * F_{0,3}(t) + P_1 * F_{1,3}(t) + P_2 * F_{2,3}(t) + P_3 * F_{3,3}(t) \quad (14)$$

In the cubic B-spline curve, four points can determine a cubic curve. Fig. 9 is the schematic diagram of the cubic B-spline curve. P_1, P_2, P_3, P_4 are four control points for fitting, and M_1 and M_2 represent respectively the midpoints of the straight lines P_0P_2 and P_1P_3 , and the start point S and end points E of the fitted curve are respectively located at one third of P_1M_1 and P_2M_2 .

In a traditional cubic B-spline curve, a uniform t value is used in the interpolation process, but in the slice data of pig body point clouds processed in the present study, the distance between the data points is not consistent. When the uniform interval t value is used to interpolate the point clouds, the experimental results show that the point clouds in the dense part of the original point clouds become even denser, while the

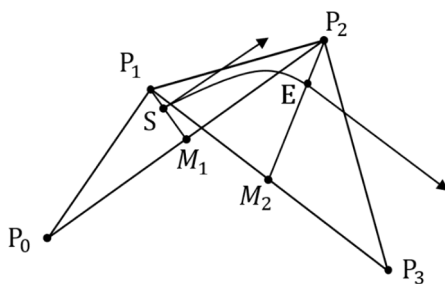


Fig. 9. Schematic diagram of cubic B-spline curve.

point clouds in the sparse part remain sparse. Consequently, the amount of computation in the repairing process will increase, and the desired repair effect cannot be achieved. To solve this problem, we propose an adaptive t -value algorithm. Specifically, set the minimum distance d between the desired point clouds, and for the fitted cubic curve g , pass four control points $P_0 = f_0(0, y_0, z_0), P_1 = f_1(0, y_1, z_1), P_2 = f_2(0, y_2, z_2), P_3 = f_3(0, y_3, z_3)$ and $t = 0, t = 1$ to calculate the start point g_0 and the end point g_1 .

$$\left\{ \begin{array}{l} g_0 = P(0) = \frac{f_0 + f_1 + f_2 + f_3}{6} \\ g_1 = P(1) = \frac{1}{6}f_1 + \frac{2}{3}f_2 + \frac{1}{6}f_3 \end{array} \right. \quad (15)$$

Use the average interval method to estimate the arc length of the curve at the data points of the fitted curve, set $t = 0.1$ to obtain 10 points on the curve of the points collected, calculate the length of the line segment between adjacent points and sum to obtain the Length. To replace the arc length of the fitting curve $\widehat{g_0g_1}$, calculate the interpolation density. Calculate the density of the complementary point Density by using formula (16). H is the point cloud dataset after hole repair, $H = \{P(t_j) | t_j = j^* \text{Density}, j \in \left[0, \frac{1-\text{Density}}{\text{Density}}\right]\}$.

$$\text{Density} = \frac{d}{\text{Length}} \quad (16)$$

In Fig. 10, (a) represents the point cloud projection after three B-spline interpolation repairs in the area to be filled, and (b) represents the complete slice projection that has been patched.

1.2.3. Point cloud downsampling

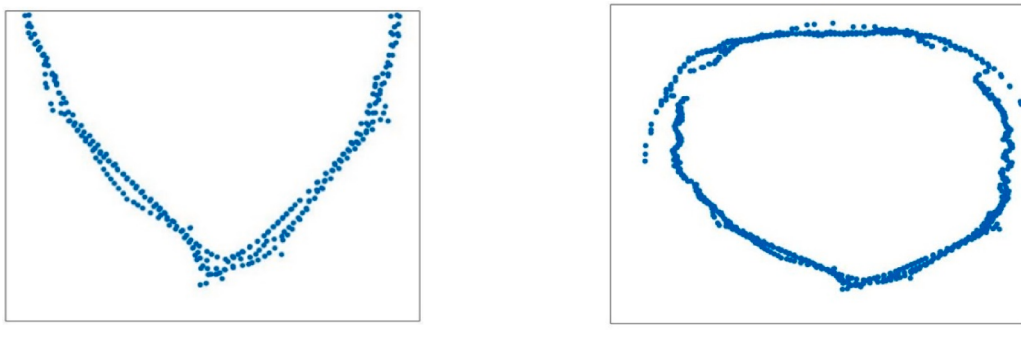
The sharp increase in the number of point clouds after hole repair brings inconvenience to the subsequent measurement work and is not conducive to data storage, so it is necessary to perform point cloud downsampling. This paper adopts the voxel filtering down-sampling algorithm. Specifically, for the target point clouds $H = \{h_1, h_2, h_3, \dots, h_m\}$, $h_i = (x_i, y_i, z_i)$, set the length of the voxel bounding box, width and height are len , wid , and high respectively, which are corresponding to the three dimensions of X, Y, and Z. For any voxel bounding box V_j , for any $h_i \in V_j, i \leq m$, there is one and only representative point $v_j(x, y, z)$ in the bounding box V_j .

$$v_j = \frac{1}{m} \sum_{k=1}^m h_k \quad (17)$$

2. Results and analyses

2.1. Analysis and comparison

For the purpose of repairing pig body point cloud holes, obtaining a complete point cloud is not only conducive to segmentation of each part



(a) Projection of repair area after hole repair

(b) Complete slice projection

Fig. 10. Point cloud projection after hole repair.

of the point clouds, but also helpful for body size measurement of pigs, especially the measurement of the thoracic circumference, rump circumference and abdominal circumference. In this paper, the abdominal circumference of the target pig is calculated by the point cloud data to verify the advantages and disadvantages of the algorithm after hole repair is completed, and comparative analysis is made among the polar coordinate transforming algorithm, the surface fitting algorithm, and the triangularization algorithm to verify the stability of the algorithm proposed in this paper.

In this paper, the point cloud data of the 1:1 pig body model is experimentally measured at first. Fig. 11 shows the collected three-dimensional pig body point cloud data with railing holes. The total number of data points is 73,217.

According to the body size measurement method [38,39], the measurement positions of abdomen, thoracic region, and rump of a target pig are determined in the 3D point cloud data, as is shown in Fig. 12, which is a schematic diagram of the measurement positions and their slices in the 3D data.

Polar coordinate transformation algorithm, surface fitting algorithm, triangularization algorithm and the algorithm proposed in this paper were respectively adopted to conduct repair experiments. Fig. 13 shows the experimental results of the four repairing algorithms, where (a), (b), (c) and (d) represent the repair effects of the above four algorithms respectively.

The abdominal circumference was calculated according to the slices at the specified position of the point clouds after hole repair, and the comparison between the results of abdominal circumference produced by various repairing algorithms and those by the manual measurement is shown in Table 1. The results in Table 1 indicate that the algorithm proposed in this paper has the smallest deviation, compared with the manual measurement in the estimation of the three aspects: thoracic circumference, abdominal circumference and rump circumference.

The posture of the model pig is fixed, so it is relatively simple to repair holes or measure the abdominal circumference. In the process of data collection of the target pigs, various postures such as turning head, lowering head, raising head, and arching back are prone to appear,

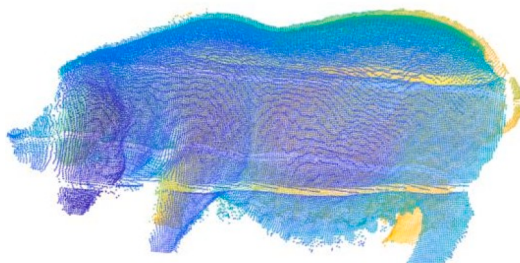


Fig. 11. Schematic diagram of the point cloud data of a pig body model.

which changes the morphologic shape of the pig body, making it difficult to accurately measure the thoracic circumference, abdominal circumference and rump circumference.

The experimental data was obtained from 20 target pigs, with each target pig providing 4 groups of 3D data in different postures through the acquisition channel in a free walking state, a total of 80 groups of point clouds with holes in the pig body. Manual measurement of abdominal circumference was performed on each target pig. In order to overcome inaccuracy of measurement, the manual measurement results were the average results measured by different stockmen for each pig. And each pig was blocked in a cage to restrict their movement, and the average measurement result were taken as the standard values in the comparisons. These 80 groups of point cloud data were repaired by using polar coordinate transformation algorithm, surface fitting algorithm, triangularization algorithm and the algorithm proposed in this paper to realize hole repair and abdominal circumference estimate. Fig. 14 shows the variation of the deviation between the estimated abdominal circumference calculated by the four algorithms and the manually measured value, and Fig. 15 shows the comparison results of the estimated abdominal circumference calculated by each algorithm and the manually measured value. Among them, the absolute average error of the four algorithms mentioned above for abdominal circumference measurement and manual measurement results were 3.32cm, 2.93cm, 5.03cm and 1.91cm respectively. Compared with the other three algorithms, the abdominal circumference value calculated by the 3D pig body point cloud repaired by the algorithm proposed in this paper is the closest to the manual measurement value, and the performance is more consistent in the abdominal circumference estimate of different 3D data for the same pig body. Compared with the other three repairing algorithms, the algorithm proposed in this paper has better stability.

2.2. Algorithm robustness test

This paper also uses cubic B-spline curve fitting algorithm to repair holes in a variety of standard animal point clouds. These standard animal point clouds are derived from Princeton Model Net and Large Geometric Models Archive at Georgia Institute of Technology. Among them, the data sets of five animals were selected: dinosaur, horse, cow, dog, and puma. Railing holes and abdominal holes for each animal point cloud were made through a random function. Fig. 16 represents the three-dimensional effect of the point cloud data used in the experiment, where (a) - (e) correspond to the standard point clouds which display the 3D effects of dinosaur, horse, cow, dog, and puma, respectively, and (f) - (j) are the point cloud data of dinosaur, horse, cow, dog, and puma with random holes.

The above four repairing algorithms were used to repair the standard animal point cloud data with random holes. Fig. 17, Fig. 18, Fig. 19 and Fig. 20 respectively represent the polar coordinate transformation

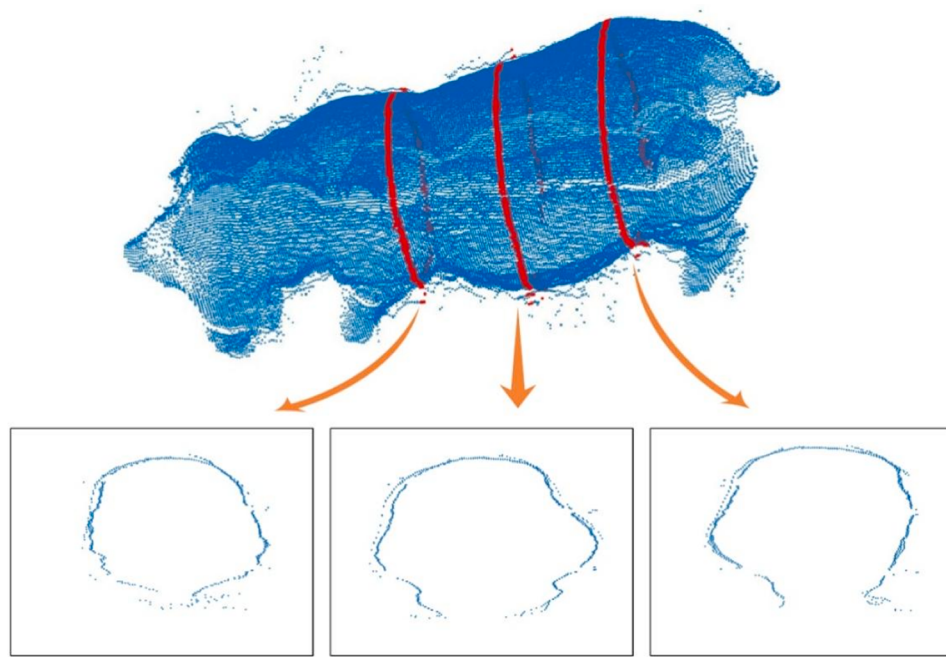


Fig. 12. Schematic diagram of the measurement positions and their slices.

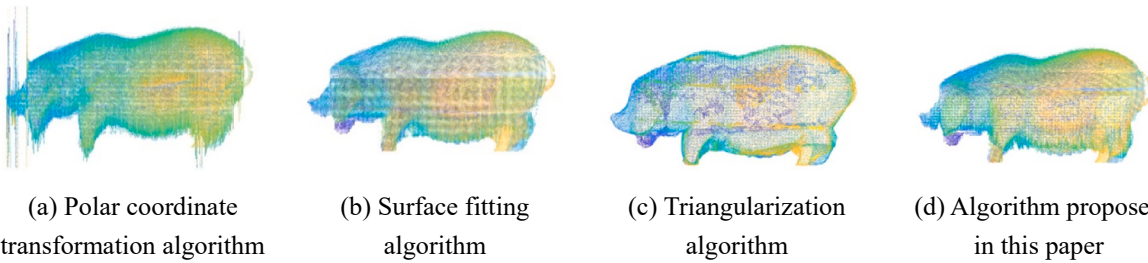


Fig. 13. Schematic diagram of the repair effects of each repairing algorithm on the pig body model.

Table 1
Three-dimensional calculated value of pig body.

Measurement methods	Thoracic circumference (cm)	Abdominal circumference (cm)	Rump circumference (cm)
Manual measurement	122.5	142.5	139.0
Unrepaired point cloud	131.9	149.5	147.3
Polar coordinate transformation algorithm	120.1	140.8	137.1
Surface fitting algorithm	121.4	150.4	267.8
Triangularization algorithm	128.1	230.2	146.7
Algorithm proposed in this paper	122.0	142.7	139.8

algorithm, surface fitting algorithm, triangularization algorithm and the algorithm proposed in this paper. The repair effect of the repairing algorithms was displayed. It can be seen that for different types of tetrapod, the hole patching effects of various repairing algorithms were uneven. Although the polar coordinate transformation algorithm had a good repair effect on the animal's abdomen, it is easily affected by the animal's limbs and head, which greatly affected the repair effect. The surface fitting algorithm can repair small-scale holes better, but the repair effect for large-scale cracks was not good enough. The

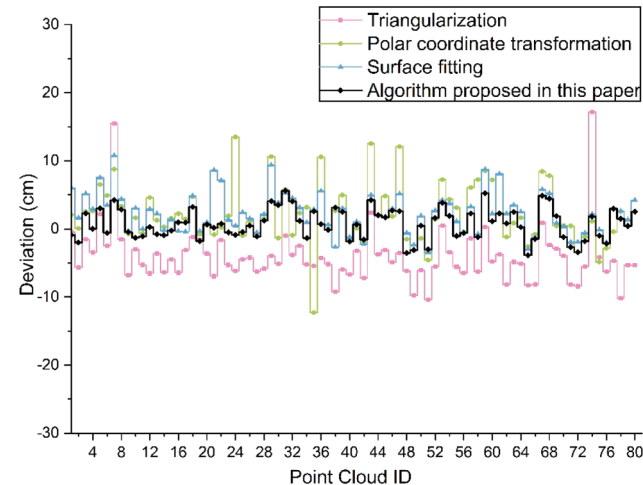


Fig. 14. Deviation changes between algorithm estimates and manual measurements.

triangularization algorithm performs well in smoothing the side point clouds, but it is suitable for the scattered point clouds, and the hole filling effect of the abdomen was not satisfactory. By contrast, the algorithm proposed in this paper had good smoothness, and the repair

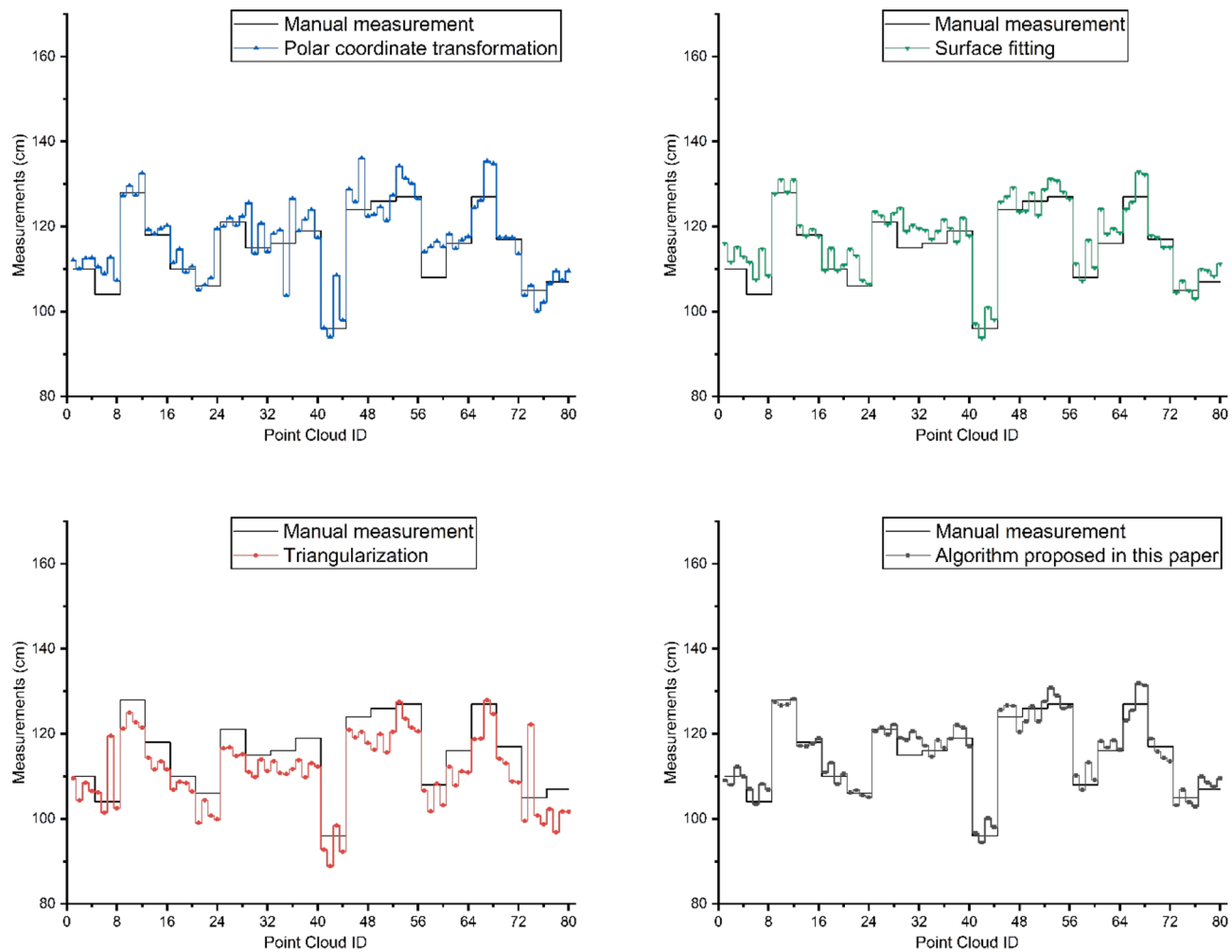


Fig. 15. Comparisons between algorithm estimates and manual measurements.

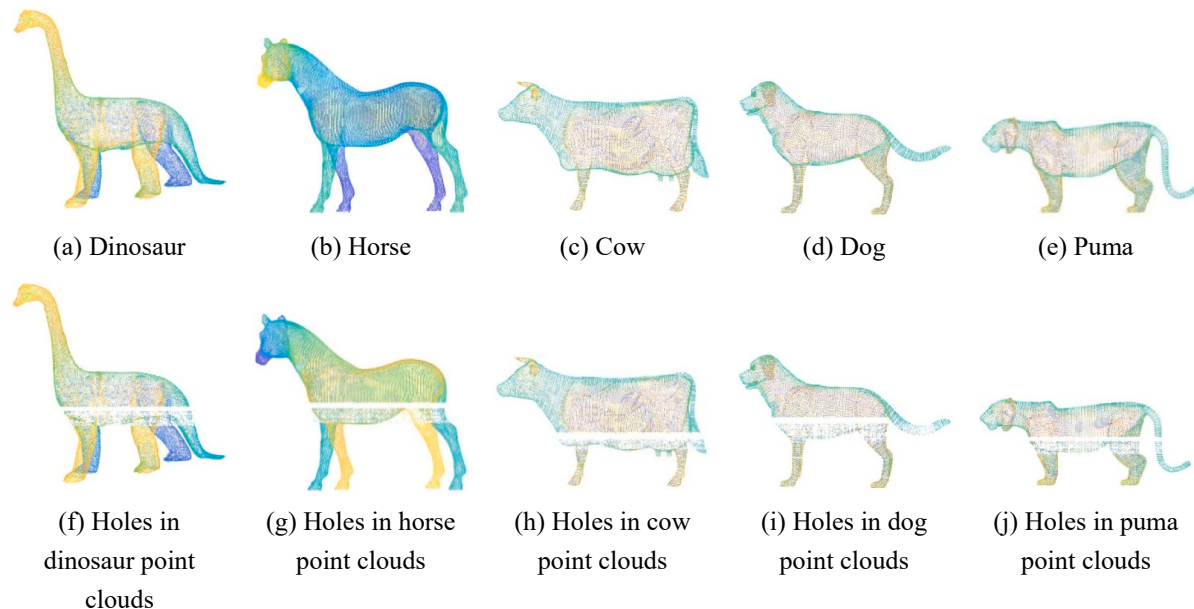
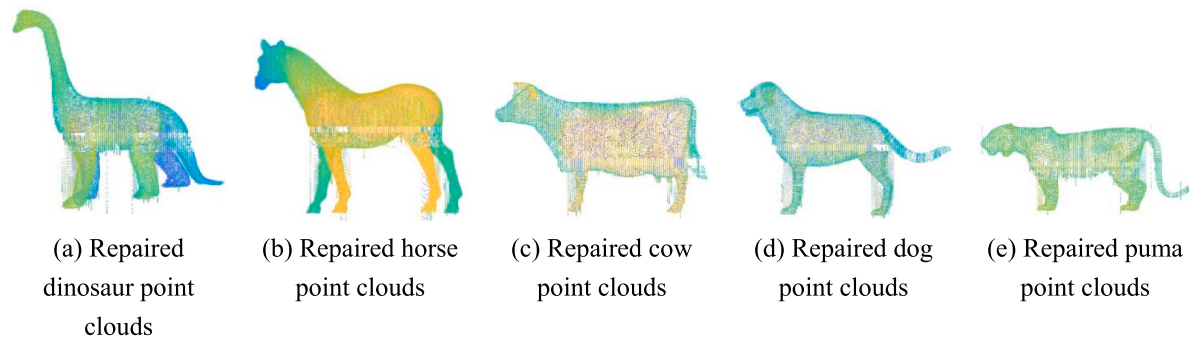
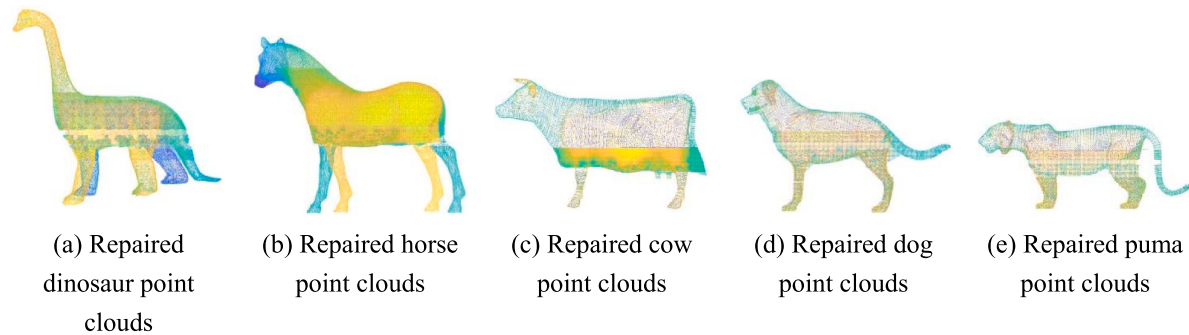
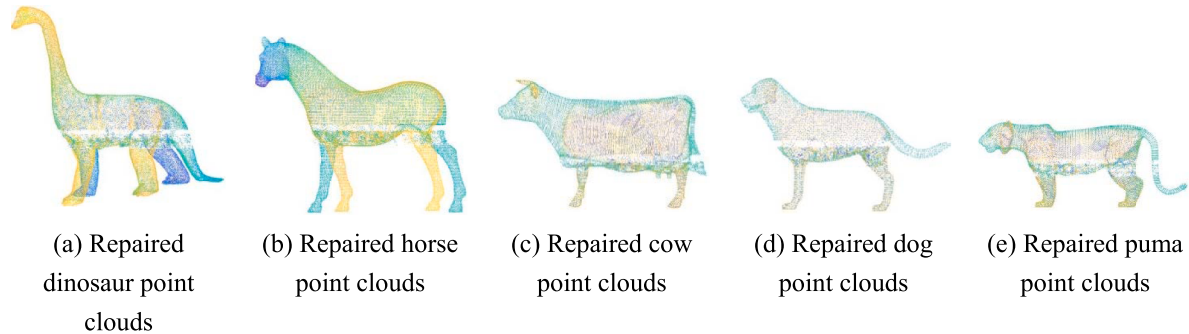
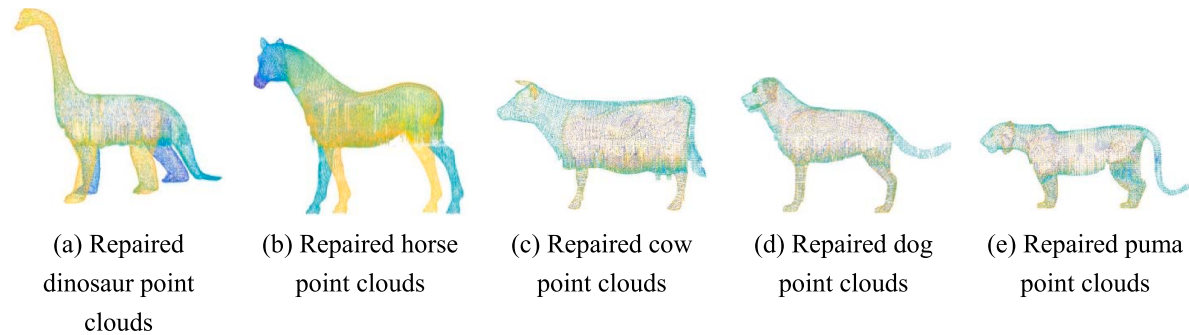


Fig. 16. Three-dimensional effects of the point cloud data

**Fig. 17.** Polar coordinate transformation algorithm.**Fig. 18.** Surface fitting algorithm.**Fig. 19.** Triangularization algorithm.**Fig. 20.** Algorithm proposed in this paper.

effect was remarkable on both sides of the animal body or the on the abdomen of the animal, which has greatly improved the repair effect on the point clouds of the tetrapod, thus showcasing good robustness.

3. Discussion

Pig body point cloud holes have different shapes in different parts. Direct repair of the global point clouds makes it difficult to ensure that each part has good versatility. Instead, by separately processing each

point cloud data with the same field characteristics, the point cloud domain characteristics of each part can be effectively restored. For example, in a pig body point cloud data set, sparse holes are likely to be found in pig ears, pig legs and pig trunks, which can be attributed to the characteristics of the depth acquisition equipment: the point clouds are dense if the equipment is fixed near, whereas the point clouds are sparse if the equipment is fixed far. Using different repairing strategies for different point clusters can have good repairing effects. The point cloud holes repairing algorithm proposed in this paper has a good repair effect on the large strip-shaped holes in the body point clouds of the standard tetrapod similar to the pig. However, the algorithm proposed in this paper does not have a good hole patching effect on pig head and on incomplete point clouds, as the pig head point clouds and the pig ear point clouds are interlaced. Therefore, when projecting longitudinal slices along the X axis, some unclosed curves that are difficult to distinguish may appear, presenting a group of scattered and irregular points. In this case, repairing will cause the pig ear point clouds to intersect with the pig head point clouds.

For the missing point clouds in non-enclosed areas, for instance, the point clouds of pig rumps are excessively incomplete due to the restriction of the depth camera visual angle. In addition, for the significantly incomplete point clouds in the non-enclosed area, the vicinity characteristics are obviously absent, so deviations are inevitable for the repair effect, which is different from the actual pig shape. Further research on repairing algorithms is essential for the incomplete point clouds.

The algorithm proposed in this paper has a limitation: when the railings happen to block the point clouds of the lowest part of the pig abdomen, the related data is missing, and the lower boundary is not the actual lower boundary to be repaired. Under the circumstances, the algorithm is no longer applicable.

4. Conclusions

- (1) Compared with traditional cubic B-spline approximate fitting and repairing algorithm, the improved hole repairing algorithm for livestock point clouds based on cubic B-spline for region defining proposed in this paper has better uniformity and approximation performance in the obtained point cloud data. The robustness of the algorithm proposed in this paper can be embodied by analyzing the repair results through the abdominal repair of the point cloud hole model data of different tetrapod animals and pigs in pig farms.
- (2) According to the experimental results, compared with other repairing algorithms, the repair results of surface fitting and the algorithm proposed in this paper are relatively close to the original point clouds in terms of visual effects. As far as the accuracy of abdominal circumference measurement is concerned, the algorithm proposed in this paper has outperformed other algorithms.
- (3) The algorithm proposed in this paper has a better repairing effect on the pig body side holes. However, the repairing effects on pig head, pig rumps and pig legs are not so satisfactory, which is quite different from the actual shape of the pig body. In the follow-up research, it is necessary to make a further study into the point cloud hole repair in the non-closed areas such as pig head and pig rumps, which is of great significance to the 3D reconstruction and modeling, thus correctly realizing visualization of pig head.

CRediT authorship contribution statement

Wen Zhikun: Conceptualization, Methodology, Software, Formal analysis, Writing – original draft. **Yu Jincheng:** Software, Methodology, Visualization, Writing – original draft. **Yin Ling:** Conceptualization, Writing – review & editing, Resources, Project administration. **Zhang**

Sumin: Resources, Data curation, Investigation. **Cai Yehao:** Software, Writing – original draft. **Liu Caixing:** Supervision, Validation. **Tian Xuhong:** Supervision, Funding acquisition.

Declaration of Competing Interest

The authors declare that they have no known competing financial interests or personal relationships that could have appeared to influence the work reported in this paper.

Acknowledgements

The authors thank Guangdong Wens Foodstuff Co., Ltd. for providing us materials to conduct the experiment. We thank everyone who has helped us to obtain data and manually measure pigs. This project is sponsored by the National Natural Science Foundation of China [32172780], Key Area R&D Plan of Guangdong Province [2019B020219001], National Engineering Research Center for Breeding Swine Industry and by the Guangzhou Key Laboratory of Intelligent Agriculture [201902010081].

Appendix A. Supplementary material

Supplementary data to this article can be found online at <https://doi.org/10.1016/j.measurement.2021.110668>.

References

- [1] J.W.M. Merks, P.K. Mathur, E.F. Knol, New phenotypes for new breeding goals in pigs, *Animal* 6 (4) (2012) 535–543, <https://doi.org/10.1017/S1751731111002266>.
- [2] Q.i. Yan, L. Ding, H. Wei, X. Wang, C. Jiang, A. Degen, Body weight estimation of yaks using body measurements from image analysis, *Measurement* 140 (2019) 76–80, <https://doi.org/10.1016/j.measurement.2019.03.021>.
- [3] Q. Wang, Y.i. Tan, Z. Mei, Computational methods of acquisition and processing of 3D point cloud data for construction applications, *Arch. Comput. Methods Eng.* 27 (2) (2020) 479–499, <https://doi.org/10.1007/s11831-019-09320-4>.
- [4] Q. Wang, M.-K. Kim, Applications of 3D point cloud data in the construction industry: a fifteen-year review from 2004 to 2018, *Adv. Eng. Inf.* 39 (2019) 306–319, <https://doi.org/10.1016/j.aei.2019.02.007>.
- [5] M. Weinmann, Preliminaries of 3D point cloud processing, in: M. Weinmann (Ed.), *Reconstruction and Analysis of 3D Scenes*, Springer International Publishing, Cham, 2016, pp. 17–38, https://doi.org/10.1007/978-3-319-29246-5_2.
- [6] K.e. Wang, H. Guo, Q. Ma, W. Su, L. Chen, D. Zhu, A portable and automatic Xtion-based measurement system for pig body size, *Comput. Electron. Agric.* 148 (2018) 291–298, <https://doi.org/10.1016/j.compag.2018.03.018>.
- [7] Y. Ling, C. Gengyuan, T. Xuhong, S. Aidong, S. Shuai, Z. Haojie, L. Shihao, Three dimensional point cloud reconstruction and body size measurement of pigs based on multi-view depth camera, *Trans. Chin. Soc. Agric. Eng. (Trans. CSAE)* 35 (23) (2019) 201–208, <https://doi.org/10.11975/j.issn.1002-6819.2019.23.025>.
- [8] E. Ozbay, A. Cinar, Z. Guler, A hybrid method for skeleton extraction on Kinect sensor data: combination of L1-Median and Laplacian shrinking algorithms, *Measurement* 125 (2018) 535–544, <https://doi.org/10.1016/j.measurement.2018.05.029>.
- [9] W. Chunxiang, H. Linwen, W. Yao, J.i. Kanghui, L. Liu, Review of hole repair in point cloud model, *Modern Manuf. Eng.* 09 (2020) 156–162, <https://doi.org/10.16731/j.cnki.1671-3133.2019.07.026>.
- [10] P. Wen, Y. Lei, M. Sun, Defective hole identification and hole-filling for 3d reconstruction mesh models, *Appl. Res. Comput.* 37 (04) (2020) 1234–1238, <https://doi.org/10.19734/j.issn.1001-3695.2018.09.0773>.
- [11] A. Kazi, A. Sausthanmath, M. S m, S.V. Gurlahosur, U. Kulkarni, Detection of holes in 3D architectural models using shape classification based Bubblegum algorithm, *Procedia Comput. Sci.* 167 (2020) 1684–1695, <https://doi.org/10.1016/j.procs.2020.03.379>.
- [12] J. Tang, Y. Wang, Y. Zhao, et al., A repair method of point cloud with big hole, in: 2017 International Conference on Virtual Reality and Visualization (ICVRV), IEEE, 2017, pp. 79–84, <https://doi.org/10.1109/ICVRV.2017.00024>.
- [13] C. Wei, Z. Zhou, Y. Dai, An efficient algorithm for defect reconstruction from 3D point cloud, in: Tenth International Conference on Graphics and Image Processing (ICGIP 2018), vol. 11069, International Society for Optics and Photonics, 2019, pp. 1106915, <https://doi.org/10.1117/12.2524243>.
- [14] N. Luo, Q. Wang, Fast self-repairing region growing surface reconstruction algorithm for unorganized point cloud data, *Int. J. Comput. Appl. Technol.* 56 (2) (2017) 121–131, <https://doi.org/10.1504/IJCAT.2017.087330>.
- [15] L.I. You-zhi, T.A.N.G. Zhi-rong, L.I.U. Ming-zhe, Algorithm of point cloud repair based on longitude and latitude grid, *Sci. Technol. Eng.* 20 (11) (2020) 4431–4435, <https://doi.org/10.3969/j.issn.1671-1815.2020.11.033>.

- [16] B. Jüttler, A. Felis, Least-squares fitting of algebraic spline surfaces, *Adv. Comput. Math.* 17 (1) (2002) 135–152, <https://doi.org/10.1023/A:1015200504295>.
- [17] Z. Yuming, Point cloud data hole-filling algorithm based on moving least square method, *Modern Electron. Technn.* 40 (21) (2017) 31–34, <https://doi.org/10.16652/j.issn.1004-373x.2017.21.008>.
- [18] Y.A.N.G. Yongqiang, L.I. Shuhong, Hole repairing algorithm for point cloud data based on least square support vector machine, *J. Jilin Univ. (Sci. Ed.)* 56 (03) (2018) 692–696, <https://doi.org/10.13413/j.cnki.jdblxb.2018.03.37>.
- [19] C. Zhang, D. Zheng, B. Wang, et al., Point cloud hole patching based on total least-square adaptive slicing, *Hydrographic Surv. Chart* 04 (2017), <https://doi.org/10.3969/j.issn.1671-3044.2017.04.013>.
- [20] S. Li, C. Ma, F. Lu, et al., Island hole repairing based on multi-directional advancing method, *China Mech. Eng.* 30 (20) (2019) 2473, <https://doi.org/10.3969/j.issn.1004-132X.2019.20.010>.
- [21] H. Yan, L. Wu, H. Chen, Hole repairing algorithm in scattered point cloud based on radial basis function, *Comput. Eng. Des.* 35 (4) (2014) 1253–1257, <https://doi.org/10.3969/j.issn.1000-7024.2014.04.026>.
- [22] W. Wang, T. Su, H. Liu, X. Li, Z. Jia, L. Zhou, Z. Song, M. Ding, Surface reconstruction from unoriented point clouds by a new triangle selection strategy, *Comput. Graph.* 84 (2019) 144–159, <https://doi.org/10.1016/j.cag.2019.08.002>.
- [23] Y. Quinsat, C. lartigue, Filling holes in digitized point cloud using a morphing-based approach to preserve volume characteristics, *Int. J. Adv. Manuf. Technol.* 81 (1-4) (2015) 411–421, <https://doi.org/10.1007/s00170-015-7185-0>.
- [24] S. Oh, A new triangular mesh repairing method using a mesh distortion energy minimization-based mesh flattening method, *Adv. Eng. Softw.* 131 (2019) 48–59, <https://doi.org/10.1016/j.advengsoft.2019.03.004>.
- [25] M. Tölgessy, M. Dekan, L. Chovanec, P. Hubinský, Evaluation of the azure kinect and its comparison to kinect V1 and kinect V2, *Sensors* 21 (2) (2021) 413, <https://doi.org/10.3390/s21020413>.
- [26] L. Shirui, L. Qi, L. Haiyang, Real-time accurate 3D reconstruction based on Kinect v2, *J. Softw.* 27 (10) (2016) 2519–2529, <https://doi.org/10.13328/j.cnki.jos.005089>.
- [27] A. Ruchay, V. Kober, K. Dorofeev, V. Kolpakov, S. Miroshnikov, Accurate body measurement of live cattle using three depth cameras and non-rigid 3-D shape recovery, *Comput. Electron. Agric.* 179 (2020) 105821, <https://doi.org/10.1016/j.compag.2020.105821>.
- [28] Y. Peng, Z. Wu, G. Cao, S. Wang, H. Wu, C. Liu, Z. Peng, Three-dimensional reconstruction of wear particles by multi-view contour fitting and dense point cloud interpolation, *Measurement* 181 (2021) 109638, <https://doi.org/10.1016/j.measurement.2021.109638>.
- [29] H. Xu, L. Yu, J. Hou, S. Fei, Automatic reconstruction method for large scene based on multi-site point cloud stitching, *Measurement* 131 (2019) 590–596, <https://doi.org/10.1016/j.measurement.2018.09.022>.
- [30] S. Zhou, X. Liu, C. Wang, B.o. Yang, Non-iterative denoising algorithm based on a dual threshold for a 3D point cloud, *Opt. Lasers Eng.* 126 (2020) 105921, <https://doi.org/10.1016/j.optlaseng.2019.105921>.
- [31] S. Li, X. Ge, H. Hu, Q. Zhu, Laplacian fusion approach of multi-source point clouds for detail enhancement, *ISPRS J. Photogramm. Remote Sens.* 171 (2021) 385–396, <https://doi.org/10.1016/j.isprsjprs.2020.11.021>.
- [32] Z. Zhang, H. Hong, X. Wang, Three and two dimensions data fusion based panoramic environment perception for space modelling, in: 2019 12th International Congress on Image and Signal Processing, BioMedical Engineering and Informatics (CISP-BMEI), IEEE, 2019, pp. 1–6, <https://doi.org/10.1109/CISP-BMEI48845.2019.8965675>.
- [33] M. Abdelazeem, A. Elamin, A. Afifi, A. El-Rabbany, Multi-sensor point cloud data fusion for precise 3D mapping, *Egypt. J. Remote Sens. Space Sci.* 24 (3) (2021) 835–844, <https://doi.org/10.1016/j.ejrs.2021.06.002>.
- [34] Z. Yao, Q. Zhao, X. Li, Q. Bi, Point cloud registration algorithm based on curvature feature similarity, *Measurement* 177 (2021) 109274, <https://doi.org/10.1016/j.measurement.2021.109274>.
- [35] N. Guo, B. Zhang, J. Zhou, K. Zhan, S. Lai, Pose estimation and adaptable grasp configuration with point cloud registration and geometry understanding for fruit grasp planning, *Comput. Electron. Agric.* 179 (2020) 105818, <https://doi.org/10.1016/j.compag.2020.105818>.
- [36] J. Liu, D. Bai, L. Chen, 3-D point cloud registration algorithm based on greedy projection triangulation, *Appl. Sci.* 8 (10) (2018) 1776, <https://doi.org/10.3390/app8101776>.
- [37] R.B. Rusu, S. Cousins, 3d is here: point cloud library (pcl), in: 2011 IEEE International Conference on Robotics and Automation, IEEE, 2011, pp. 1–4, <https://doi.org/10.1109/ICRA.2011.5980567>.
- [38] T. Liu, G. Teng, W. Fu, et al., Extraction algorithms and applications of pig body size measurement points based on computer vision, *Trans. Chin. Soc. Agric. Eng.* 29 (2) (2013) 161–168, <https://doi.org/10.3969/j.issn.1002-6819.2013.02.023>.
- [39] K. Wang, H. Guo, W. Liu, et al., Extraction method of pig body size measurement points based on rotation normalization of point cloud, *Trans. Chinese Soc. Agric. Eng.* 33 (1) (2017) 253–259, <https://doi.org/10.11975/j.issn.1002-6819.2017.z1.038>.